

Biosynthesis of elliptical hematite microparticles and their photocatalytic performance

Bashir Ahmmad^{1*}, Kensaku Kanomata¹, Fumihiko Hirose¹, Junichi Kurawaki², and Takahiro Ohkubo³

¹Graduate School of Science and Engineering, Yamagata University, Yonezawa 992-8510, Japan
E-mail: arima@yz.yamagata-u.ac.jp, kanomata@yz.yamagata-u.ac.jp, fhirose@yz.yamagata-u.ac.jp

²Department of Chemistry & Bioscience, Graduate School of Science and Engineering, Kagoshima University, Kagoshima 890-0065, Japan

E-mail: kurawaki@sci.kagoshima-u.ac.jp

³Department of Chemistry, Graduate School of Science and Technology, Okayama University, Okayama 700-8530, Japan

E-mail: ohkubo@cc.okayama-u.ac.jp

*Corresponding author

Submitted 15 July 2013; accepted in final form 6 May 2014

Abstract

A green synthesis method of α -Fe₂O₃ microparticles has been developed using the extract of green tea (*camellia sinensis*) leaves. The as-prepared microparticles were characterized by SEM, TEM, XRD, XPS, UV-visible spectroscopy, and N₂ adsorption analysis. The crystallized microparticles were elliptical in shape with a diameter and length of 1 μ m and 2 μ m, respectively. The photocatalytic activity of the microparticles was evaluated by the amount of hydroxyl radical formation under visible light irradiation detected by fluorescence spectroscopy. The as-prepared α -Fe₂O₃ showed similar photocatalytic activity as the commercial α -Fe₂O₃ in terms of hydroxyl radical formation. The microparticles were easy to separate from the aqueous suspension by gravity settling after water treatment. A plausible mechanism for the formation of α -Fe₂O₃ microparticles was suggested.

Keywords: iron oxide, hydroxyl radical, green tea, green synthesis.

1. Introduction

Semiconductor photocatalysis is one of the recognized advanced physicochemical processes for solving existing environmental problems such as waste water containing organic compounds (Hoffmann, Martin, Choi, and Bahnemann, 1995; Ahmmad, Kusumoto, Ikeda, Somekawa and Horie, 2007; Valenzuela, Bosch, Jiménez-Becerrill, Quiroz and Páez, 2002). TiO₂ is the most studied materials among various semiconductor photocatalysts but due to large band gap (3.2 eV), TiO₂ requires UV-light for activation (Fujishima and Honda, 1972) which covers only 5% of solar light. On the other hand, Fe₂O₃ having a band gap of 2.2 eV can be activated by visible-light irradiation and it has been found to be highly active catalyst for the photodegradation of organic pollutants. For example, Karunakaran and Senthilvelan (2006) reported Fe₂O₃ photocatalytic oxidation of aniline to azobenzene with sustainable catalytic activity. Pal and Sharon (1998) reported the photocatalytic decomposition of salicylic acid with visible light in an oxygenated aqueous suspension of colloidal α -Fe₂O₃ particles. About 10-20 ppm of this organic compound is degraded

within 1 h of irradiation, depending upon the initial salicylic acid concentration. Although Fe₂O₃ can efficiently mineralize a great number of organic pollutants, the recovery of the photocatalyst powder from treated water is still an obstacle to widely extending application as the photocatalyst particles must be filtered prior to the discharge of the treated water. To exclude the separation procedure, the immobilization of the photocatalysts on certain supporting materials such as glass, fiber or stainless steel has been frequently adopted as reviewed by Byrne et al. (1998). Unfortunately, a significant loss in the contact area between the immobilized photocatalyst and light limits its efficiency in the photocatalytic degradation of the organic substrates (Rachel, Subrahmanyam, and Boule, 2002). On the contrary, the photocatalyst powder in suspension systems enjoys an attractive advantage of good contact with light, thus leading to a relatively high quantum yield. Therefore, a possible practical alternative would be to maintain the supported catalyst in a suspension form. When the fluidized photocatalyst is ferromagnetic, magnetic separation is an excellent method of separation

after the reaction. Since $\alpha\text{-Fe}_2\text{O}_3$ is weakly ferromagnetic, it is not practical to recover using a magnet (Kostedt, Byrne and Mazyck, 2010). Gravity settling is another useful and easy separation method after water treatment if the particles are large enough. However, if the particle size becomes larger the surface area decreases and also catalytic activity decreases. Therefore, it is challenging to produce $\alpha\text{-Fe}_2\text{O}_3$ microparticles which are easy separable by gravity settling, low cost and highly photoactive. Micro-sized $\alpha\text{-Fe}_2\text{O}_3$ photocatalysts have been reported by some researchers (Xuan, Chen, Hao, Jiang, Gong, Hua, and Chen, 2008; Zhang, Sui, Gong, Su, and Qu, 2007; Gu, Li, Wang, Li, Sun, Xu, and Zhang, 2009). However, most of these methods usually require special equipment, high temperature, templates or substrate. These add difficulties in prefabrication as well as post-removal of the templates or substrate and the process usually introduces impurities. Moreover, the toxic byproducts immersing from these chemical reactions are often potentially harmful to the environment (Tang, Wang, Zhuo, Ge, and Cui, 2006). On the other hand, use of biological organisms such as microorganisms, plant extract or plant biomass could be an alternative to chemical and physical methods for the generation of metal or metal oxide nanoparticles in an eco-friendly manner (Leonard, Ahmmad, Okamura, and Kurawaki, 2011). To date, plant mediated synthesis is limited solely to metal nanoparticles though bacteria assisted biosynthesis of metal oxides nanoparticles has been applied by some researchers (Jha and Prasad, 2010; Zhou, He, Ma, Wang, Zhang, Yan, Tian et al., 2009). Recently, we reported biosynthesis of $\alpha\text{-Fe}_2\text{O}_3$ nanoparticles using the extract of green tea (Ahmmad, Leonard, Islam, Kurawaki, Muruganandham, Ohkubo, and Kuroda, 2013). Here we report, the preparation of highly crystallized and highly pure elliptical shaped $\alpha\text{-Fe}_2\text{O}_3$ microparticles by a simple and one-step hydrothermal method, using the extract of green tea leaves.

2. Experiment

2.1. Materials and methods

Fresh green tea leaves were collected from the local garden of Kagoshima, Japan. $\text{FeCl}_3 \cdot 6\text{H}_2\text{O}$ (99.0%) and NaOH (95%) were purchased from Wako (Japan). Terephthalic acid

(98%) was received from Sigma-Aldrich Chemicals Ltd. (Japan). All these chemicals were used as received and for all experimental works, doubly deionized water was used.

2.2. Preparation of microparticles

Two g of dry green tea leaves were put into 150 ml water and heated at 80 °C for 20 min on a hot plate. The solution was filtered and stocked at 10 °C. In a beaker, 5 g of $\text{FeCl}_3 \cdot 6\text{H}_2\text{O}$ was dissolved in 30 ml of green tea-extract and then 30 ml of distilled water was added for the hydrothermal process. The solution was transferred to an autoclave which was heated at different temperature (100 °C to 180 °C) for 13 h under ambient pressure. The autoclave was cooled to room temperature and the product was washed with water and dried at 80°C or calcined at 350 °C for 2 h under air atmosphere. The effect of time of the hydrothermal process on the size and morphology of microparticles was investigated up to 48 hours while keeping the temperature constant at 140 °C.

2.3. Characterization of microparticles

The size and morphology of the microparticles were analyzed by a field-emission scanning electron microscope (FE-SEM) (Hitachi, S-4100H) and a transmission electron microscope (TEM) (JEOL, JEM-3010 VII, operating at 300 kV). Crystal structure identification was made by X-ray diffraction (XRD) using a PANalytical Advance X-ray diffractometer with $\text{CuK}\alpha$ radiation. The chemical nature was performed by X-ray photoelectron spectroscopy (XPS) (Shimadzu, ESCA-1000) using $\text{MgK}\alpha$ X-ray as the excitation source and C1s (284.6 eV) as the reference line. The purity of the sample was further confirmed by energy dispersive X-ray spectrometer (EDX, Philips, XL-30cp) attached to the cold field SEM. The UV-visible diffuse reflectance spectra were recorded using a spectrophotometer. Brunaur-Emmet-Teller (BET) surface area was determined using a BELSORP-max (BEL Japan) nitrogen adsorption apparatus.

2.4. Determination of photocatalytic activity

The quantitative analysis of hydroxyl radical ($\cdot\text{OH}$) formed on the photocatalyst surface under visible light irradiation was carried out by fluorescence spectroscopy using terephthalic acid,

which readily reacted with $\cdot\text{OH}$ to produce highly fluorescent product, 2-hydroxyterephthalic acid. The fluorescence intensity of this 2-hydroxyterephthalic acid is known to be proportional to the amount of $\cdot\text{OH}$ formed (Ishibashi et al., 2000). About 60 mg of as-prepared $\alpha\text{-Fe}_2\text{O}_3$ microparticles were added to 50 mL of 5×10^{-4} M terephthalic acid solution in 2×10^{-3} M NaOH, and then visible light irradiation to the solution was started. A xenon lamp (Ushio, 500 W) was used as a visible light source with an UV cut-off filter. For the measurement of the active oxidative species (mainly corresponding to $\cdot\text{OH}$ produced by $\alpha\text{-Fe}_2\text{O}_3$ microparticles), a fluorophotometer (Shimazu, RF-5300PC) was used. Sampling was performed in every 15 min. Solutions, after filtration through a 0.20- μm membrane filter, were analyzed by a fluorescence spectrophotometer. The hydroxylation product of terephthalic acid, 2-hydroxyterephthalic acid, gave

a peak at the wavelength of about 425 nm by the excitation with the wavelength of 315 nm.

3. Results and discussion

3.1 Properties

The size and morphology of the as-synthesized $\alpha\text{-Fe}_2\text{O}_3$ were examined by SEM and TEM analysis. The SEM images (Figure 1a, b, c) of as-prepared $\alpha\text{-Fe}_2\text{O}_3$ demonstrate that the products consist of elliptical microparticles with uniform size and no aggregation of the oval microparticles is observed. As shown in the TEM image of Figure 1d, the microparticles are solid (without hollow cores). However, there are some pores in the particles which were further analyzed by N_2 adsorption analysis discussed later in this manuscript. The diameter and length of microparticles were estimated to be 1 μm and 2 μm , respectively.

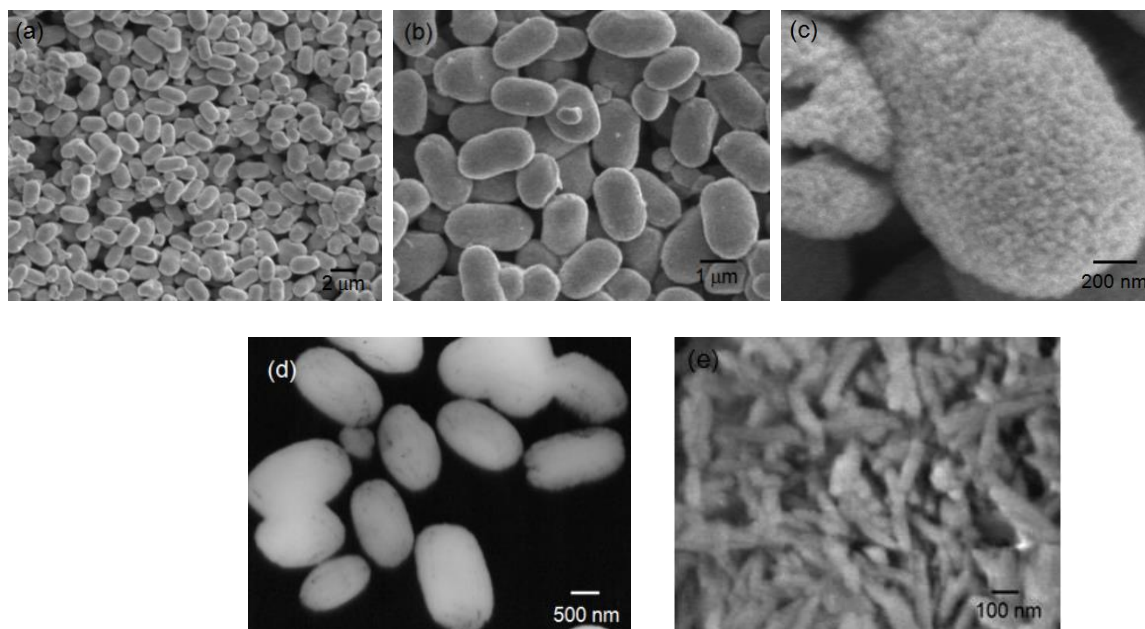


Figure 1 SEM (a, b, c) and TEM (d) images of as prepared $\alpha\text{-Fe}_2\text{O}_3$ microparticles; (e) is the SEM image of samples collected after 3 h of hydrothermal process.

The XRD pattern of as-prepared and calcined α - Fe_2O_3 microparticles are shown in Figure 2a. All of the peaks can be easily indexed to rhombohedral α - Fe_2O_3 with lattice parameters $a = 0.5028$ and $c = 1.373$ nm (Space group $R3c$), which are in agreement with the reported values (JCPDS 86-0550). No other peaks for impurities were observed. There was no shift or appearance of new peak in XRD after calcination of as-prepared sample. It was found that below 100°C , the reaction did not proceed and no product was found. At 100°C very small amount of product was obtained which shown no recognizable XRD peaks. The product prepared at 120°C shows clear XRD peaks for hematite and with increasing the temperature from 120 to 180°C , the sharpness of the XRD peaks for hematite was increased (data not shown). These observations imply that the highly crystalline α - Fe_2O_3 are feasible to produce by the present method at low temperature and calcinations process is not a necessary step to enhance the crystallinity of the product. The

average crystal size (t) for the as-prepared α - Fe_2O_3 microparticles was calculated using Debye-Scherrer's equation, $t = 0.89\lambda/\beta\cos\theta$, where, λ is the X-ray wavelength, β is the full width at half maximum of diffraction line, and θ is the diffraction angle of the XRD spectra. The average crystal size was calculated to be around 43 nm, which is in agreement with the SEM image of Figure 1c. These nanometer sized particles aggregate together to form the oval-shaped microparticles.

The effect of time of hydrothermal process on the size and morphology of microparticles was investigated upto 48 h keeping temperature constant at 140°C . The product collected after 3 h was of rod shaped nanoparticles (Figure 1e) and that after 6 h was of elliptical microparticles which XRD peaks could be indexed to $\text{Fe}_8\text{O}_8(\text{OH})_8\text{Cl}_{1.35}$ and hematite, respectively (Figure 2b). There was no considerable change in the particles size or morphology upto 48 h of hydrothermal process.

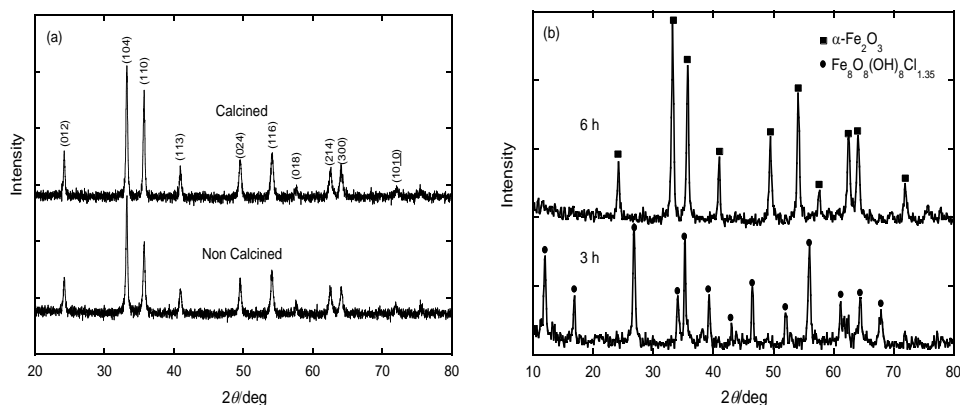


Figure 2 XRD patterns for calcined and non-calcined as prepared α - Fe_2O_3 microparticles (a), samples collected after 3 h and 6 h of hydrothermal process (b)

In order to confirm the oxidation state of Fe in α - Fe_2O_3 , XPS was used to examine the as-prepared samples. Figure 3a shows representative XPS spectra of the hematite. Elemental analysis confirmed the presence of Fe, C and O elemental signatures. No other elemental signals were detected in the XPS spectra. The photoelectron peaks at 711 and 725 eV are the characteristic doublets of Fe $2p_{3/2}$ and $2p_{1/2}$ core-level spectra of iron oxide, respectively. Also, the corresponding

satellite peak located at 719 eV, approximately 8 eV higher than the main Fe $2p_{3/2}$ peak of α - Fe_2O_3 , is clearly distinguishable and does not overlap either the Fe $2p_{3/2}$ or Fe $2p_{1/2}$ peak. It can be solely attributed to the presence of Fe^{3+} ions of α - Fe_2O_3 , as the binding energy values are too high to be any other oxide species of iron (Zhao et al., 2006). In addition, the O1s core levels show the dominant oxide peaks at around 529.9 eV, which are in good agreement with the literature values of α - Fe_2O_3 (Li,

Liu and Dong, 2007). The Fe 2p and O 1s core levels indicate that the valence states of Fe and O are +3 and -2, respectively. To further prove the purity of the final product, EDX spectra of the as-prepared samples were measured. Also, as shown in Figure 3b, the EDX spectrum shows only iron and oxygen elements in 2:3 ratio which implies that the sample is highly pure Fe₂O₃. The porosity of the as-synthesized α -Fe₂O₃ microparticles was analyzed by the nitrogen adsorption-desorption isotherms and corresponding pore-size distribution (PSD) obtained by Barrett-Joyner-Halenda (BJH) method as shown in Figure 4a. The product shows type II isotherms indicating the presence of micropores and the surface area of as-prepared

sample was found to be 7.0 m²/g, which is the same value as the commercial α -Fe₂O₃ (surface area of 7 m²/g).

The UV-vis diffuse reflectance spectra of as-prepared and heated samples are shown in Figure 4b. The absorption spectra exhibit a broad absorption in the visible region, extending into the UV, with a tail extending to 570 nm. The optical absorption bands in visible and UV region are attributed to the transition in crystal field and the charge transfer processes and the difference in the absorbance is due to difference in their morphology and size.

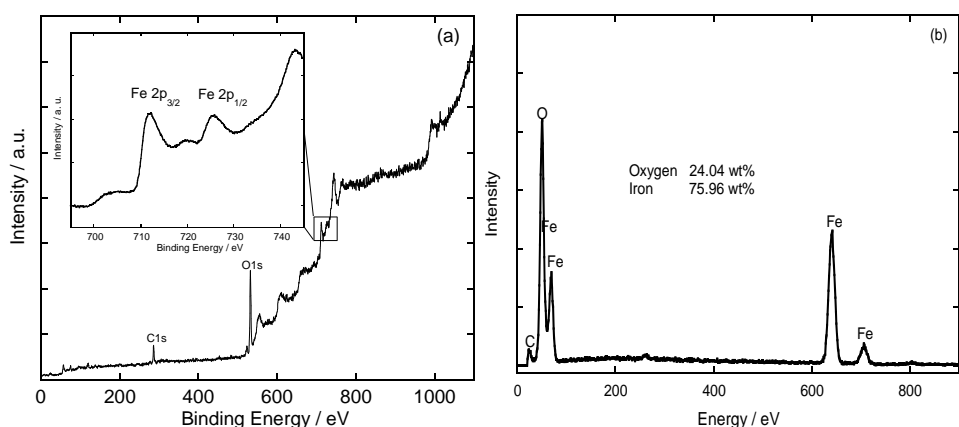


Figure 3 XPS spectra (a), EDX spectra (b) of α -Fe₂O₃ microparticles

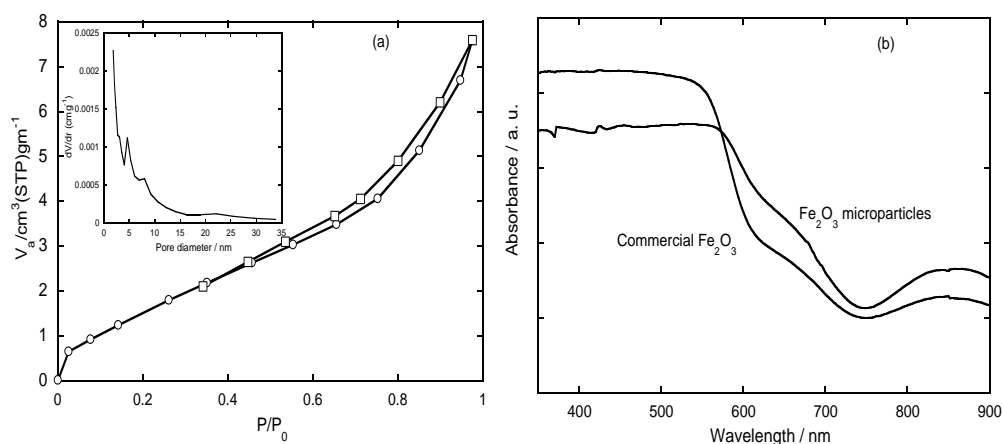


Figure 4 Nitrogen adsorption-desorption isotherm and PSD curve (a) and UV-vis diffuse reflectance spectra (b) for as prepared α -Fe₂O₃ microparticles

3.2 Formation mechanism of microparticles

Generally, the formation of microstructure relates to the two primary mechanisms: the aggregation growth process and the Ostwald ripening process. Crystal growth by aggregation can occur by random aggregation and/or oriented attachment mechanism, while the Ostwald ripening process involves the growth of larger crystals at expense of smaller ones (Wang et al., 2008). We assume that both of the mechanisms are involved in the formation of Fe_2O_3 microparticles. The overall hydrolysis reaction of FeCl_3 in hydrothermal process can be expressed as follows:



Previously, we reported formation mechanism of nanoparticles mediated by green tea extract (Ahmmad et al., 2013). It was shown that the main component of green tea Epigallocatechin gallate (EGCG) could form complex with hydrolysed species such as $\text{Fe}(\text{OH})_2^+$. With increasing temperature of hydrothermal process a phase transformation occurs forming the primary particles. Wan, Yan, Wang, Li, and Zou (1995) showed that when large content of Cl^- ion is present in the started solution, the nucleation is

relatively slow, leading to fewer Fe_2O_3 nuclei. Once the iron oxide nuclei are formed, they grow larger to minimize surface energy. We assume that the nanorods of $\text{Fe}_8\text{O}_8(\text{OH})_8\text{Cl}_{1.35}$ are formed in the first step of aggregation because we detected them after 3 h of hydrothermal process as suggested by XRD (Figure 2b) and SEM image (Figure 1e). The formation of rod shaped nanoparticles is also reported by Wang et al. (2008) during the formation of microsphere from FeCl_3 solution by hydrothermal process. In the second step of aggregation growth the newly formed primary particles are driven by the Ostwald ripening process and nanorods become oval structures in micrometer size. When the hydrothermal process was further prolonged, a phase transformation occurred resulting in the forming of hematite Fe_2O_3 as evident from the elliptical microstructures found in the sample after 6 h of hydrothermal process (data not shown). In the Ostwald ripening process larger particles are formed by aggregation of smaller subunits and therefore the surface of such particles are not smooth but rough. The surfaces of microparticles in this work are also rough as evident from the high-magnification SEM images (Figure 1c). This result supports the involvement of Ostwald ripening mechanism in the formation of microparticles.

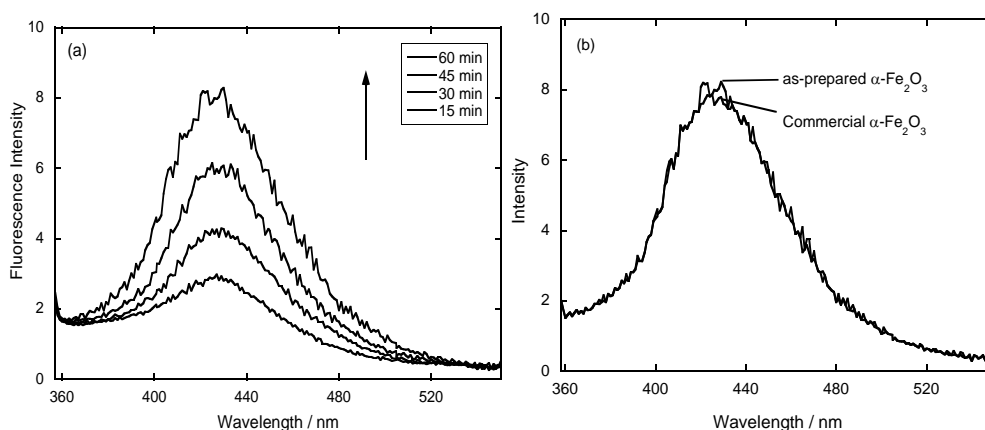


Figure 5 Fluorescence spectra for as-prepared $\alpha\text{-Fe}_2\text{O}_3$ at different irradiation-time (a) and a comparison of photocatalytic activity for as-prepared and commercial $\alpha\text{-Fe}_2\text{O}_3$ after 1 h of irradiation (b)

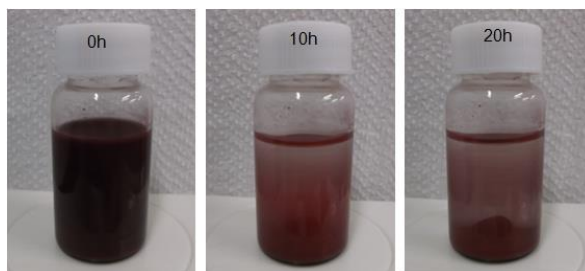


Figure 6 Digital photos of suspension at different time interval after the photocatalytic reactions

3.3 Photocatalytic Performance

The fluorescence emission spectrum (excitation at 315 nm) of terephthalic acid solution was measured every 15 min during illumination. It was found that the fluorescence intensity increases with increasing illumination time (Figure 5a). Consequently, we could conclude that the amount of $\cdot\text{OH}$ formed at the $\alpha\text{-Fe}_2\text{O}_3$ interfaces was in proportional to the light illumination time obeying zero-order reaction rate kinetics. Based on the report by Khan, Anwar, and Ahmad (1995), it was reasonable to assume that photogenerated O_2^- , $\text{HO}_2\cdot$ and H_2O_2 did not interfere with the reaction between $\cdot\text{OH}$ and terephthalic acid. Moreover, the generated spectrum had the identical maximum wavelength with that of 2-hydroxyterephthalic acid. These results suggested that fluorescent products formed using Fe_2O_3 were due to the specific reaction between $\cdot\text{OH}$ and terephthalic acid. Figure 5b shows the plots of fluorescence intensity of the as-prepared $\alpha\text{-Fe}_2\text{O}_3$ microparticles and the commercial $\alpha\text{-Fe}_2\text{O}_3$ nanoparticles after 1h of visible light irradiation ($\lambda > 400$ nm). It is shown that the as-prepared $\alpha\text{-Fe}_2\text{O}_3$ has similar photocatalytic activity to the commercial $\alpha\text{-Fe}_2\text{O}_3$ in terms of hydroxyl radical formation. After the photocatalytic reaction, we observed that the particles settled down from the suspension in 20 h as shown in Figure 6.

4. Conclusion

We successfully prepared $\alpha\text{-Fe}_2\text{O}_3$ microparticles by a combination of hydrothermal and biosynthesis method. The environmentally friendly method is low cost, one-step which gives highly pure and highly crystallized $\alpha\text{-Fe}_2\text{O}_3$ microparticles. The as-prepared microparticles show similar photocatalytic activity to commercial $\alpha\text{-Fe}_2\text{O}_3$ nanoparticles in terms of hydroxyl radical

formation under visible light irradiation. The microparticles are naturally separated from the aqueous suspension after 20 hours.

5. Acknowledgements

This research was supported by Improvement of Research Environment for Young Researchers from the Ministry of Education, Culture, Sports, Science and Technology-Japan. The authors also wish to thank Mr. Masao Arima of Kagoshima Prefecture for providing fresh green tea leaves.

6. References

- Ahmmad, B., Kusumoto, Y., Ikeda, M., Somekawa, S., & Horie, Y. (2007). Photocatalytic hydrogen production from diacids and their decomposition over mixtures of TiO_2 and single walled carbon nanotubes. *J. Adv. Oxid. Technol.*, 10(2), 415-420.
- Ahmmad, B., Leonard, K., Islam, M. S., Kurawaki, J., Muruganandham, M., Ohkubo, T., & Kuroda, Y. (2013). Green synthesis of mesoporous hematite ($\alpha\text{-Fe}_2\text{O}_3$) nanoparticles and their photocatalytic activity. *Adv. Power. Tehnol.*, 24(1), 160-167.
- Byrne, J. A., Eggins, B. R., Brown, N. M. D., McKinney, B., & Rouse, M. (1998). Immobilisation of TiO_2 powder for the treatment of polluted water. *Appl. Catal. B: Environ.*, 17, 25-36.
- Fujishima, A., & Honda, K. (1972). Electrochemical photocatalysis of water a semiconductor electrode. *Nature*, 238, 37-38. doi:10.1038/238037a0.
- Gu, J., Li, S., Wang, E., Li, Q., Sun, G., Xu, R., & Zhang, H. (2009). Single-crystalline $\alpha\text{-Fe}_2\text{O}_3$ with hierarchical structures:

- controllable synthesis, formation mechanism and photocatalytic properties. *J. Solid. State. Chem.*, *182*, 1265-1272.
- Hoffmann, M. R., Martin, S. T., Choi, W., & Bahnemann, D. W. (1995). Environmental applications of semiconductor photocatalysis. *Chem. Rev.*, *95*(1), 69-96.
- Ishibashi, K., Fujishima, A., Watanabe, T., & Hashimoto, K. (2000). Detection of active oxidative species in TiO₂ photocatalysis using the fluorescence technique. *Electrochem. Commun.*, *2*, 207-210.
- Jha, A. K., & Prasad, K. (2010). Biosynthesis of metal and oxide nanoparticles using *Lactobacilli* from yoghurt and probiotic spore tablets. *Biotechnol. J.*, *5*(3), 285-291. doi: 10.1002/biot.200900221.
- Karunakaran, C., & Senthilvelan, S. (2006). Fe₂O₃-photocatalysis with sunlight and UV light: Oxidation of aniline. *Electrochem. Commun.*, *8*(1), 95-101.
- Khan, H. M., Anwar, M., & Ahmad, G. (1995). Effect of temperature and light on the response of an aqueous coumarin dosimeter. *J. Radioanal. Nucl. Chem. Lett.*, *200*, 521-527.
- Kostedt, I. V., Byrne, H. E., & Mazyck, D. W. (2010). A high surface area magnetic photocatalyst with controlled pore size. *Environ. Prog. Sustain. Energy*, *29*(1), 10-16.
- Leonard, K., Ahmmad, B., Okamura, H., & Kurawaki, J. (2011). In situ green synthesis of biocompatible ginseng capped gold nanoparticles with remarkable stability. *Colloids. Surf. B Biointerfaces*, *82*(2), 391-396.
- Li, L., Chu, Y., Liu, Y., & Dong, L. (2007). Template-free synthesis and photocatalytic properties of novel Fe₂O₃ hollow spheres. *J. Phys. Chem., C*, *111*, 2123-2127.
- Pal, B., & Sharon, M. (1998). Photocatalytic degradation of salicylic acid by colloidal Fe₂O₃ Particles. *J. Chem. Technol. Biotechnol.*, *73*(3), 269-273.
- Rachel, A., Subrahmanyam, M., & Boule, P. (2002). Comparison of photocatalytic efficiencies of TiO₂ in suspended and immobilised form for the photocatalytic degradation of nitrobenzenesulfonic acids. *Appl. Catal. B: Environ.*, *37*(4), 301-308.
- Tang, B., Wang, G., Zhuo, L., Ge, J., & Cui, L. (2006). Facile Route to α -FeOOH and α -Fe₂O₃ nanorods and magnetic property of α -Fe₂O₃ nanorods. *Inorg. Chem.*, *45*, 5196-5200.
- Valenzuela, M. A., Bosch, P., Jiménez-Becerrill, J., Quiroz, O., & Páez, A. I. (2002). Preparation, characterization and photocatalytic activity of ZnO, Fe₂O₃ and ZnFe₂O₄. *J. Photochem. Photobiol., A*, *148*, 177-182.
- Wan, L., Yan, S., Wang, X., Li, Z., & Zou, Z. (2011). Solvothermal synthesis of monodisperse iron oxides with various morphologies and their applications in removal of Cr(VI). *Crys. Eng. Comm.*, *13*, 2727-2733.
- Wang, D., Song, C., Zhao, Y., & Yang, M. (2008). Synthesis and characterization of monodisperse iron oxides microspheres. *J. Phys. Chem., C*, *112*, 12710-12715.
- Xuan, S., Chen, M., Hao, L., Jiang, W., Gong, X., Hua, Y., & Chen, Z. J. (2008). Preparation and characterization of microsized FeCO₃, Fe₃O₄ and Fe₂O₃ with ellipsoidal morphology. *Magn. Magn. Mater.*, *320*(3-4), 164-170.
- Zhang, X., Sui, C., Gong, J., Su, Z., & Qu, L. (2007). Preparation and formation mechanism of different α -Fe₂O₃ morphologies from snowflake to paired microplates, dumbbell and spindle microstructures. *J. Phys. Chem., C*, *111*, 9049-9054.
- Zhao, Y. M., Li, Y. H., Ma, R. Z., Roe, M. J., McCartney, D. G., & Zhu, Y. Q. (2006). Growth and characterization of iron oxide nanorods/nanobelts prepared by a simple iron-water reaction. *Small*, *2*(3), 422-427.
- Zhou, W., He, W., Ma, J., Wang, M., Zhang, X., Yan, S., Tian, X., Sun, X., & Han, X. (2009). Biosynthesis of mesoporous organic-inorganic hybrid Fe₂O₃ with high photocatalytic activity. *Mater. Sci. Eng., C*, *29*, 1893-1896.